GROUP MEAN DIFFERENCES OF VOXEL AND SURFACE OBJECTS VIA NONLINEAR AVERAGING

Shun Xu[1], *Martin Styner*[1,2], *Brad Davis*[1,3], *Sarang Joshi*[1,3], *Guido Gerig*[1,2] *

The University of North Carolina
Departments of [1]Computer Science, [2]Psychiatry, [3]Radiation Oncology
Chapel Hill, NC 27599. xushun@cs.unc.edu

ABSTRACT

Building of atlases representing average and variability of a population of images or of segmented objects is a key topic in application areas like brain mapping, deformable object segmentation and object classification. Recent developments in image averaging, i.e. constructing an image which is central within the population, focus on unbiased atlas building with nonlinear deformations. Groupwise nonlinear image averaging creates images which appear sharper than linear results. However, volumetric atlases do not explicitely carry a notion of statistics of embedded shapes. This paper compares population-based linear and non-linear image averaging on 3D objects segmented from each image and compares voxel-based versus surface-based representations. Preliminary results suggest improved locality of group average differences for the nonlinear scheme, which might lead to increased significance for hypothesis testing. Results from a clinical MRI study with sets of subcortical structures of children scanned at two years with follow-up at four years are shown.

1. INTRODUCTION

The construction of brain atlases is central to the understanding of the variabilities of brain anatomy. Most research has been directed towards the development of 3D brain atlases using image mapping algorithms [1, 2] that can map and transform a single brain atlas onto a population. In this paradigm the atlas serves as a deformable template and the nonlinear transformations encode the variability of the population. Most recent work [3, 4] of nonlinear unbiased atlas building avoids the bias introduced by template selection. Further, pairwise deformations are replaced by simultaneous groupwise estimations of the unbiased atlas and the transformations [5, 6].

Principal component analysis (PCA) has been applied directly to the high dimensional dense deformation fields or to the control points of the free-form deformation to study the variabilities of the deformation fields[7]. Robustness of this conventional linear method is highly reduced due to insufficient training in practical settings[8]. Linear surface shape statistical methods can also be used to calculate average shapes and major modes of variation, such as PDM [9] and SPHARM [10]. This Euclidean framework has to be replaced by a nonlinear Riemannian space framework when applied to nonlinear medial shape models [11]. But statistical shape properties derived from nonlinear deformation fields of atlases have not been sufficiently studied.

The difference between linear and nonlinear voxel-based atlas building schemes clearly showed improved sharpness of the nonlinear method [6]. However, its advantage for statistical analysis of shapes and hypothesis testing between groups has not yet been sufficiently explored.

This paper describes work in progress that explores statistical properties of shape populations averaged via nonlinear deformations obtained by unbiased atlas building. Preliminary results are shown as comparison of shape averaging via linear and nonlinear deformations, and as exploration of the potentials of nonlinear schemes in group discrimination and localization of population differences.

2. EXPERIMENTAL DESIGN

In order to compare group differences of linear v.s. nonlinear shape averages, our shape analysis methods can be divided into four steps. First, 3D affine transformation and nonlinear unbiased groupwise registration[4] are applied to two groups of grey level brain images, respectively. Information of all transformations are retained. Second, binary voxel representation of subcortical structures are extracted from the same two groups of brain images, using semi-automatic user-supervised segmentation. Applying the corresponding transformations retained from step one to these binary segmentations and averaging them result in linear and nonlinear average images. Third, parameterized surface representations of anatomical brain structures are established based on the binary segmentations in step two. Linear and nonlinear shape

*We would like to thank Matthieu Jomier for the computation of the original brain deformation maps. The datasets were provided by the UNC Autism center and NIH grant RO1 MH61696. This research is supported by the NIH NIBIB grant P01 EB002779 and the UNC Neurodevelopmental Disorders Research Center HD 03110.

averages are derived by applying the affine transformations and the 3D deformation fields retained in step one to surface points followed by averaging the resulting transformed objects. Finally, group differences are studied by both volumetric and surface comparisons.

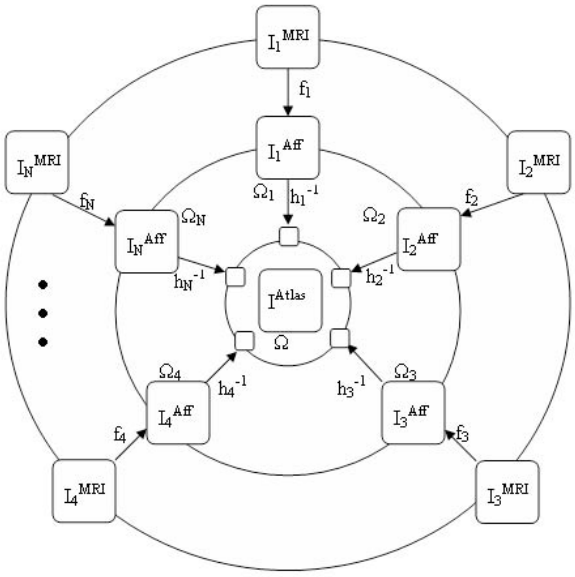

Fig. 1. Linear and nonlinear construction framework applied to MRI brain images.

The construction framework depicted in Figure1 produces affine transformations $\{f_i\}_{i=1}^N$ such that $f_i : I_i \rightarrow I_i^{Aff}$, where $\{I_i\}_{i=1}^N$ are a population of N individual MRI images and $\{I_i^{Aff}\}_{i=1}^N$ are their corresponding affinely-transformed counterparts. Nonlinear diffeomorphic mappings $h_i : \Omega \rightarrow \Omega_i$ are then estimated to deform each I_i^{Aff} into an unbiased atlas I^{Atlas}[4, 6], where $\Omega \subset \mathbf{R}^3$ and $\Omega_i \subset \mathbf{R}^3$ are the coordinate systems of I^{Atlas} and I_i^{Aff} respectively. Since each h_i is a diffeomorphism[4], its inverse $h_i^{-1} : \Omega_i \rightarrow \Omega$ exists and can be calculated.

In this study, two groups of 5 cases are selected over Time1 (2 years of age) and Time2 (4 years of age) from our autism study database. The above framework was then applied to obtain the linear affine transformations $\{f_i\}_{i=1}^N$ and nonlinear deformations $\{h_i^{-1}\}_{i=1}^N$, where $N = 5$.

We started with gray-level MRI image deformations to obtain $\{f_i\}_{i=1}^N$ and $\{h_i^{-1}\}_{i=1}^N$, and then applied them to binary voxel and surface segmentations. Thus we can study shape variability and group differences in different aspects and make comparison, which will be illustrate in the following sections.

3. VOXEL-BASED REPRESENTATION AND PROCESSING

In this section we describe how to obtain linear and nonlinear probability maps. Anatomical structures were first segmented from MRI data using user-supervised segmentation by geodesic snakes and then represented as binary voxel representations. Each of the N MRI data I_i corresponds to T binary segmentations $\{B_{ij}\}_{j=1}^T$ of T brain structures.

Each of the NxT segmentations B_{ij} were affinely transformed into B_{ij}^{Aff} by f_i using trilinear interpolation, respectively. Averaging B_{ij}^{Aff} over i gives us population probability maps for affine transformations, as shown in Figure2 (a). We then continued to deform B_{ij}^{Aff} into B_{ij}^{def} using the deformation field h_i^{-1}. Averaging B_{ij}^{def} over i gives us population probability maps after nonlinear deformations, as shown in Figure2 (b).

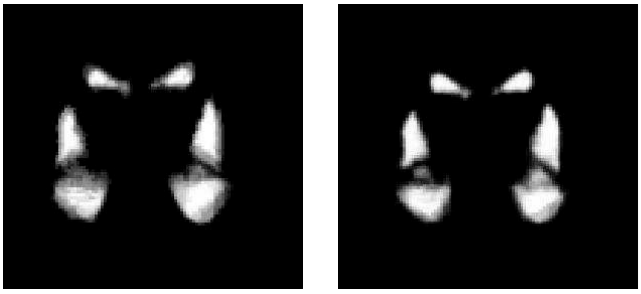

Fig. 2. Coronal view of combined objects illustrating ventricles, caudates, and amygdalae. Left: Probability map of linearly transformed segmentations of subcortical brain structures. Right: Probability map of nonlinearly deformed segmentations.

Note that the deformation fields $\{h_i^{-1}\}_{i=1}^N$ are obtained via fluid deformation between grey level volumetric images but without explicit notion of object boundaries. These deformation fields are then applied to the embedded binary segmentations to validate the quality of atlas building. The result in Figure 2 shows that linear averaging of voxel objects creates blurry probability maps, whereas nonlinear averages appear sharper.

4. SURFACE-BASED REPRESENTATION AND PROCESSING

Voxel-based image averaging does not result in an explicit representation of average object boundaries and does not directly express surface variability of anatomical structures. In this section, we therefore apply the set of linear and nonlinear transformations to object surface representations.

After voxel segmentation, shapes were processed by an analysis pipeline that includes surface extraction and parametrization using spherical harmonics[12, 10]. This parametric

boundary description is called SPHARM. Using a uniform icosahedral subdivision of the spherical parametrization gives us Point Distribution Models (PDM). PDM point correspondence over the whole population is defined by surface points with equivalent surface parameterizations.

In our study, each of the MRI images I_i has T boundary models $\{S_{ij}\}_{i=1}^{T}$, while each shape S_{ij} has $M = 1442$ boundary points $\{P_{ijk}\}_{k=1}^{M}$ derived from the SPHARM descriptor. $\{P_{ijk}\}_{i=1}^{N}$ are corresponding points from parametrization, which means point k of shape j corresponds to each other invariant to individual i. In this surface averaging process, original surface correspondences are propagated through all stages of deformations and can be used for object averaging.

The affine transformations f_i were applied to the points $\{\{P_{ijk}\}_{k=1}^{M}\}_{j=1}^{T}$ individually. Grouping all the M mean points $\bar{P}_{jk}^{Aff} = \frac{1}{N}\sum_{i=1}^{N} P_{ijk}^{Aff}$ gives us a linear shape average $\bar{S}_j$ of structure j. Similarly, nonlinear deformation fields were applied to all NxTxM points accordingly, and a nonlinear shape average $\bar{S}^{def}$ was obtained. Note that $\{f_i\}_{i=1}^{N}$ and $\{h_i^{-1}\}_{i=1}^{N}$ applied to surface points are obtained via affine transformation and fluid deformation between grey level volumetric images.

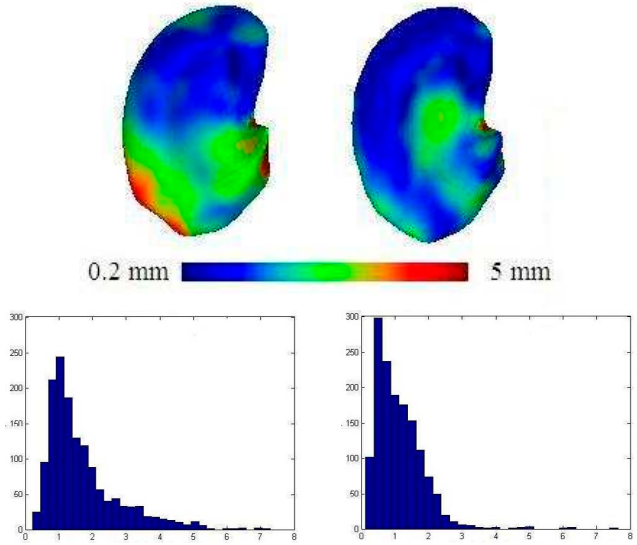

Fig. 3. Top: Colormaps of standard-deviation of surface points ploted on average shapes. Top left: Colormap of STDs of linearly transformed surface points. Top right: Colormap of STDs of nonlinearly deformed surface points. Bottom: Histograms of STDs correspond to the shape above. Putamen is chosen as an illustration example.

Similar to a representation of a fuzzy boundary in voxel-based processing as a measure of "sharpness" of the population model, variability of a population is expressed by calculating the standard-deviation of each surface point.

In Figure 3, we see that the shape on the right depicts more blue region, which implies variability of nonlinearly deformed surface corresponding points is in generally smaller; while on the left the image is more with green and red color, which implies bigger variability for linearly transformed surface corresponding points. While we gain intuitions by looking at the colormap of the STDs, the corresponding histogram and the table of statistical data are shown in Figure 3 and Table 1.

Standard deviation statistics of putamen at Time1:		
	Affine	Nonlinear
Mean	1.6816	1.1261
50 percentile	0.3311	0.1807
85 percentile	0.3759	0.2141

Table 1. Statistical data of the two histograms of standard deviation shown in Figure 3. The data shows smaller variability of surface points in the nonlinear case.

5. GROUP DIFFERENCE ANALYSIS

In this section we compares voxel-based and surface-based representations and explores group differences obtained via linear and nonlinear shape averaging.

5.1. Volumetric Analysis Between Groups

The result in Figure2 shows that nonlinear averages of voxel objects appear sharper than averages done in a linear scheme. In order to assess linear and nonlinear methods in group difference comparison, we compute probabilistic distance between two groups Time1 v.s. Time2 by the following probability overlap measure[13]:

$$POV(A,B) = 1 - \frac{\int |P_A - P_B|}{2\int P_{AB}}$$

Probabilistic distance: Time1 v.s. Time2				
	L. Caud	R. Caud	L. Put	R. Puta
Affine	0.85391	0.92314	0.79608	0.89028
Nonlinear	0.88659	0.92457	0.83059	0.85069

Table 2. Distances between probability maps of Time1 and Time2 , as shown in Figure2. Caudate and Putamen are chosen as illustration examples.

As shown in table 2, distances of affine and nonlinear probability maps are very close. By looking at these numbers of global probabilistic measurement, it is difficult to gain information of localization or intuitive conception. Volumetric analysis seems inefficient to address our problem of group comparison by different approaches, which motivates analysis via an explicit object representation.

5.2. Shape Mean Difference Analysis Between Groups

With the goal of exploring whether the nonlinear scheme shows potentials to improve group discrimination, we compares the differences between group means calculated by both linear and nonlinear averaging.

We applied the processing described in section 4 to two populations over two time points, respectively, and we obtain for each time point the surface-based group mean after affine registrations and that after nonlinear deformations. Comparing the group mean differences over time gives results on the left and middle in Figure 4. On the other hand, the voxel-based scheme described in section 3 gives us linear and nonlinear probability maps, out of which we applied thresholding and surface extraction to obtain the surfaces of average voxel objects. Comparing them over time gives the result on the right in Figure 4.

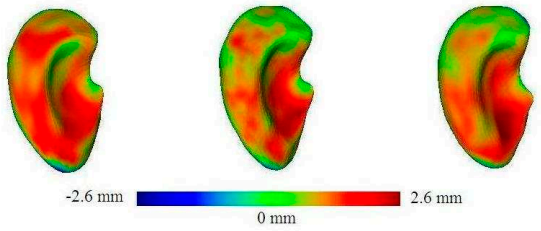

Fig. 4. Groupwise average model comparison shown for caudate and putamen. Left column: mean difference between Time1 and Time2 after affine transformation. Middle: mean difference between Time1 and Time2 after nonlinear diffeomorphic deformation. Right column: difference of boundary models extracted from threshold of Time1 and Time2 probability maps.

Figure 4 illustrates the mean shape difference color-coded on the surface. The illustrations suggest that mean differences are more distributed for the affine registrations and more concentrated at specific regions for nonlinear. The average surface after nonlinear deformation (middle) and surface of average voxel object (right) appear similar, as both represent objects obtained by nonlinear averaging but using a surface-based versus voxel-based processing.

The above preliminary results are very interesting and suggested improved locality of group average differences for the nonlinear scheme, which intrigues our continuing work of hypothesis testing.

6. DISCUSSION

In order to gain insights into the potential of a nonlinear scheme in improving localization of group differences, this paper discusses the comparison of group mean differences of voxel-based and surface-based objects via linear and nonlinear averaging. We started with two populations represented as MRI images and its unbiased atlases, then applied the affine registrations and nonlinear diffeomorphic deformations to binary voxel and surface segmentations of subcortical structures, and studied the population mean differences. We make use of the notion of statistics of the embedded shapes to study the properties of nonlinear atlas deformation fields, and explore its potentials in group discrimination. Our findings suggest better localization of group mean differences for nonlinear schemes and they provide ample motivation for the future shape difference hypothesis testing in the non-linear deformation setting.

7. REFERENCES

[1] A. W. Toga P. M. Thompson, "A framework for computational anatomy," *Computing and Visualization in Science*, , no. 5, pp. 13–34, 2002.

[2] U. Grenander M. I. Miller, "Computational anatomy: An emerging discipline," *Quarterly of Applied Mathematics*, vol. 56, pp. 617–694, 1998.

[3] B. Avants J.C. Gee, "Symmetric geodesic shape averaging and shape interpolation," in *ECCV Workshops CVAMIA and MMBIA*, 2004, pp. 99–110.

[4] S. Joshi B. Davis M. Jomier G. Gerig, "Unbiased diffeomorphic atlas construction for computational anatomy," in *NeuroImage*, 2004, vol. 23, pp. S151–S160.

[5] C. J. Twining T. Cootes S. Marsland V. Petrovic R. Schestowitz C. J. Taylor, "A unified information-theoretic approach to groupwise non-rigid registration and model building," in *IPMI*, 2005, pp. 1–14.

[6] P. Lorenzen M. Prastawa B. Davis G. Gerig E. Bullitt S. Joshi, "Multi-model image set registration and atlas formation," in *MedIA*, 2005, to appear.

[7] D. Rueckert A. F. Frangi and J. A. Schnabel, "Automatic construction of 3d statistical deformation models using non-rigid registration," in *MICCAI*, 2001, pp. 77–84.

[8] Z. Xue D. Shen B. Karacali and C. Davatzikos, "Statistical representation and simulation of high-dimensional deformations: Application to synthesizing brain deformations," in *MICCAI*, 2005.

[9] T. F. Cootes C. J. Taylor D. H. Cooper J. Graham, "Active shape models - their training and application," in *Computer Vision and Image Understanding*, 1995, pp. 38–59.

[10] Ch. Brechbüehler G. Gerig O. Kübler, "Parametrization of closed surfaces for 3d shape description," in *CVIU*, 1995, pp. 154–170.

[11] P.T. Fletcher C. Lu S.M. Pizer S. Joshi, "Principal geodesic analysis for the study of nonlinear statistics of shape," in *IEEE TMI*, 2004, vol. 23, pp. 995–1005.

[12] M. Styner J. A. Lieberman D. Pantazis G. Gerig, "Boundary and medial shape analysis of the hippocampus in schizophrenia," in *MedIA*, 2003, pp. 197–203.

[13] G. Gerig M. Jomier M. Chakos, "Valmet: A new validation tool for assessing and improving 3d object segmentation," in *MICCAI*, 2001, pp. 516–528.